Organic-free synthesis of nanostructured SnO2 thin films by chemical solution deposition

Aleksej Zarkov, Andrius Stanulis, Lina Mikoliunaite, Andrei N. Salak, Aivaras Kareiva

PII: S0040-6090(18)30072-5
DOI: https://doi.org/10.1016/j.tsf.2018.01.056
Reference: TSF 36455

To appear in: *Thin Solid Films*

Received date: 24 July 2017
Revised date: 25 January 2018
Accepted date: 28 January 2018

Please cite this article as: Aleksej Zarkov, Andrius Stanulis, Lina Mikoliunaite, Andrei N. Salak, Aivaras Kareiva , Organic-free synthesis of nanostructured SnO2 thin films by chemical solution deposition. The address for the corresponding author was captured as affiliation for all authors. Please check if appropriate. Tsf(2017), https://doi.org/10.1016/j.tsf.2018.01.056

Organic-free synthesis of nanostructured SnO_2 thin films by chemical solution deposition

Aleksej Zarkov[1,*], Andrius Stanulis[2], Lina Mikoliunaite[1], Andrei N. Salak[3], Aivaras Kareiva[1]

[1]*Faculty of Chemistry and Geosciences, Vilnius University, Naugarduko 24, LT-03225 Vilnius, Lithuania*

[2]*Institute of Chemistry, Center for Physical Sciences and Technology, Sauletekio av. 3, LT-10257 Vilnius, Lithuania*

[3]*Department of Materials and Ceramic Engineering/CICECO, University of Aveiro, 3810-193 Aveiro, Portugal*

*Corresponding author: E-mail: aleksej.zarkov@chf.vu.lt; +37062190153.

Abstract

Novel synthetic approach for preparation of single phase porous SnO_2 thin films with controllable grain size and porosity has been developed. The entire process require neither organic solvents nor addition of any complexing agent. The thin films were deposited using the spin coating technique from an aqueous solution prepared by dissolving tin(II) oxalate in hydrogen peroxide. X-ray diffraction analysis showed that the deposited films are single-phase and their crystallite size increases as the annealing temperature is increased from 300 to 800 °C. It was also found that the films exhibit a preferred (110) orientation of the crystallites. Scanning electron microscopy and atomic force microscopy were employed for the estimation of thickness and surface morphological features of the films. Thickness of the films after 10 deposition cycles was about 160 nm. Roughness of the films increased with the annealing temperature increasing. It has been found from the UV-Vis spectrometry measurements that the films are highly transparent in visible spectral range. The optical band gap was determined to be in the range from 3.86 to 4.00 eV depending on the annealing temperature.

Keywords: thin films, tin dioxide, chemical solution deposition, spin coating.

1. Introduction

Tin dioxide (stannic oxide) is one of the most important wide band gap semiconducting materials that has been extensively investigated over the past decades. SnO_2 has a tetragonal rutile structure with two tin and four oxygen atoms per unit cell. The ideally stoichiometric SnO_2 is an insulator, however, the real SnO_2 structure contains oxygen vacancies, which make this material an oxygen-deficient n-type semiconductor. Tin(IV) oxide attracts scientific interest since it combines important physical properties such as a high optical transparency in the visible spectrum, a low electrical resistance, good chemical and thermal stability [1]. During the last decade, transparent conducting SnO_2 has found great technological applications as electrode material for solar cells [2], resistive gas sensors [3, 4], photocatalysis [5] and self-cleaning coatings [6]. Furthermore, SnO_2 films have already been utilized as stable high-rate anodes for lithium-ion batteries [7, 8] and protective oxygen barrier layer on aluminum doped zinc oxide films [9].

Low-dimensional systems such as thin films, two-dimensional heterostructures and surface layers attract a considerable attention because of their chemical, physical, and functional properties different from those of the conventional bulk materials. Consequently, a large number of studies are devoted to nanostructured thin films due to their wide range of applications. The influence of crystallite size and porosity on the material properties is especially remarkable for polycrystalline thin films [10]. The efficiency of optoelectronic devices could be considerably improved using porous transparent film electrodes instead of dense ones because of much higher surface area of the formers [11]. Considering the gas sensor applications, the sensing mechanism of SnO_2 is categorized as a surface-control type, in which the grain sizes, surface states and oxygen adsorption quantities have important roles. High surface area is one of the key factors which promote gas diffusion and enhance material transportation processes, thus shortening the response time and improving sensitivity of the sensors [12].

Both pure and doped SnO_2 thin films have recently been synthesized using various techniques such as spray pyrolysis [13], atomic layer deposition [14], RF sputtering [15], thermal evaporation [16],

pulsed laser deposition [17] and chemical vapor deposition [18]. Due to simplicity and low cost, the chemical solution deposition technique can be the best alternative for the synthesis of sub-micrometer thin SnO_2 films. Moreover, this technique allows to prepare large area coatings. Alcohol-based solutions prepared by dissolving either Sn(II) chloride or Sn(IV) chloride in ethanol [19, 20] or methanol [21] are most frequently used for synthesis of sol-gel derived SnO_2 films. However, elimination of corrosive to metals chlorides together with organic additives from the film occurs at elevated temperatures. The preparation of SnO_2 thin films via aqueous sol-gel directly using SnC_2O_4 as a starting material and triethanolamine/citric acid as a stabilizing agents has been reported [22-24]. The decomposition of Sn(II) oxalate by hydrogen peroxide and further complex formation with citric acid was successfully applied for deposition of SnO_2 films [25] and more complex ternary oxides [26]. However, according to the thermogravimetric analysis of the utilized precursors, in both aforementioned methods the complete decomposition of organic-inorganic framework occurs at 500–550 °C. Presence of chelating agents and organic solvents may lead to the contamination with elemental carbon if annealing temperature is insufficient for their removal from the final product. As a result, residues of organic species or inorganic carbon may influence physical properties of the films such as transparency. As-deposited films that contain no organic stabilizers do not require high temperature decomposition procedure. Thus, either amorphous or nanostructured SnO_2 films can be obtained using organic-free Sn(IV) peroxo precursor. Moreover, low process temperatures appear to be very promising for deposition on flexible or temperature sensitive substrates.

In the present work, we report on synthesis, characterization and some physical properties of the SnO_2 thin films with sub-micrometer thickness on SiO_2/Si and fused silica substrates. The entire process require neither organic solvents nor addition of any complexing agent. The oxidative decomposition of Sn(II) oxalate allows to avoid a presence of counter-ions in the precursor solution. The proposed method is simple, fast and cost-effective. It is capable of producing crack-free,

polycrystalline, single phase and porous thin films with controllable grain size and porosity at comparatively low temperatures.

2. Experimental

2.1. Deposition of thin films

A precursor solution was synthesized by the following procedure. An appropriate amount of tin(II) oxalate (SnC_2O_4, Sigma-Aldrich, 98%) was dissolved in 30% (w/w) hydrogen peroxide under continuous stirring and heating. Afterwards, prepared solution was filtered through 0.2 μm membrane filter and diluted to a certain volume with deionized water. The concentration of Sn ions in the final solution was 0.25 M.

Multilayered SnO_2 films were prepared on the SiO_2/Si and fused silica substrates by spin coating technique using a SCS P6700 spin coater. Prior to the deposition, the substrates were cleaned with a mixture of concentrated sulfuric acid and hydrogen peroxide followed by washing with deionized water. Several drops of the precursor solution were placed onto the substrates and spin coated for 30 s @ 3000 rpm (acceleration was 1000 rpm/s). A sample with as-deposited wet film was put on a hot plate and kept for about 5 min at 300 °C. The complete deposition-drying cycle was repeated a certain number of times prior to a final annealing in a furnace at different temperatures for 2 h (1 °C/min).

Small amounts of the solution used for the film deposition were dried and the obtained powders were then annealed together with the films.

2.2. Characterization

The thermal decomposition of the precursor solution was analyzed by the thermogravimetric and differential scanning calorimetry (TG-DSC) using a Perkin Elmer STA 6000 Simultaneous Thermal Analyzer. Dried samples of about 5–10 mg were heated from 25 to 900 °C at a heating rate of 5 °C/min in a dry flowing air (20 mL/min). The crystal structure and crystallite size of the obtained samples were characterized by methods of X-ray diffraction (XRD) using a PANalytical X'Pert Powder diffractometer (Ni-filtered Cu Kα radiation, PIXcel^{1D} detector). The deposited films were

measured in a grazing incidence X-ray diffraction (GIXRD) mode using a Multi-Purpose Sample Stage. The XRD patterns were collected with a grazing angle of 2° in the range from 20 to 80 degrees with a step of 0.02° and a counting time of about 7 s per step. The XRD measurements of the powder samples were performed using a Spinner Sample Stage (Bragg-Brentano geometry, the 2Theta angular range of 20–80^o, step 0.02^o, 0.5 s per step, a sample rotation of 4 s^{-1}). The obtained diffraction data were refined by the Rietveld method using the FULLPROF suite in the profile matching mode [27].

The average crystallite size (τ) was calculated by Scherrer equation:

$$\tau = \frac{0.9\lambda}{B\cos\theta} \quad (1)$$

where λ is the X-ray wavelength, B is the full width at half maximum (FWHM) of a diffraction peak and θ is the Bragg angle. The morphology of the films was characterized using a Hitachi SU-70 field-emission scanning electron microscope (FE-SEM). For the surface characterization of deposited films, an atomic force microscope (AFM) BioScope Catalyst from Bruker was used. The tapping mode was employed and sharpened silicon nitride (DNP-S type) AFM probes were applied. Transmittance spectra were recorded in a wavelength range from 190 to 1100 nm using an Analytik Jena Specord 200 plus UV-vis spectrometer.

3. Results and discussion

3.1. Synthesis of precursor solution

Chemical reactions between hydrogen peroxide, oxalic acid and metal oxalates were previously described in literature [28-30]. Under heating conditions in the presence of hydrogen peroxide, tin(II) oxalate decomposes with evolution of the appropriate amounts of CO_2 and H_2O. At the same time, Sn^{2+} ions are oxidized to Sn^{4+} with a formation of stannic acid. Thereby, such an approach allows to eliminate presence of organic chelating agents and counter-ions such as Cl^-, which are usually present when tin chloride is used as a starting material. The only elements present in precursor solution are Sn, O and H.

3.2. Thermal analysis

The thermal decomposition behavior of dried SnO_2 precursor solution was investigated by simultaneous TG-DSC measurements in order to display decomposition steps (see Fig. 1). It is evident that thermal degradation occurs in two main steps. The first step with a mass loss of about 3% is observed in the temperature range from 30 to 150 °C and ascribed to the removal of adsorbed water. The second gradual mass loss peaked at ~250 °C is attributed to dihydroxylation process of terminal –OH groups. At the temperatures above 600 °C, the residual mass is nearly constant and further changes are non-significant. The overall weight loss was found to be about 10%.

3.3. XRD analysis

Fig. 2 represents the GIXRD patterns of the SnO_2 coatings processed on SiO_2/Si substrates at different annealing temperatures. It can be seen that crystalline phase forms already after annealing at 300 °C. All the diffraction peaks matched well with the tetragonal SnO_2 structure (space group $P4_2/mnm$ [31]); no diffraction reflections arising from by-products such as SnO or Sn_3O_4 have been observed. The diffraction peaks were very broad although with the regular shape indicating that the broadening is mainly caused by nanocrystalline nature of the films. An increase of the annealing temperature from 300 to 800 °C resulted in sharpening of the diffraction peaks suggesting a growth of the crystallites. It was found from a comparison of the FWHM values of the diffraction peaks observed in the XRD patterns of the films and the powders prepared from the same SnO_2 precursor solutions and then annealed at the same temperatures that the values for the films are regularly higher than the respective ones for the powders. Such a difference may imply that the deposited films are stressed because of the film-substrate misfits.

Indeed, the lattice parameters calculated from the Rietveld analysis were found to be essentially different for the films and the powders annealed at equal conditions. Fig. 3 shows results of the Rietveld refinements for powders and film both annealed at 800 °C. Fig. 4 demonstrates the lattice parameters *a* and *c* of the tetragonal SnO_2 phase as a function of the annealing temperature. One can see that the *a*-parameter of the SnO_2 powders slightly increases as the annealing temperature is increased while the *c*-parameters is constant within the experimental error. The lattice parameter

values of the powders are very close to those reported by McCarthy and Welton (a: 4.7382 Å, c: 3.1871 Å) for the synthetic cassiterite [31] (ICDD 00-041-1445). It is also seen from Fig. 4 that both *a*- and *c*-parameters of the films annealed at temperatures above 400 °C are regularly larger than those of the respective powders. Moreover, the lattice parameters of the films demonstrate a rather strong dependence on annealing temperature: the *a*-parameter increases and the *c*-parameter decreases as the annealing temperature is increased. At the same time, the corresponding values of the lattice parameters of the SnO_2 films formed either on SiO_2/Si substrates or on fused silica substrates turned out to be equal within the experimental error. The XRD patterns of the films are different from those of the powders not only in terms of the angle positions of the respective reflections but also in respect of their relative intensities. The integral intensities of the strongest reflections (110), (101) and (211) of a polycrystalline SnO_2 [31] (ICDD 00-041-1445) relate to each other as 100:75:57. A similar ratio of the intensities was observed in the XRD patterns of the SnO_2 powders studied in this work. In the patterns of the SnO_2 films deposited either on SiO_2/Si substrates or on fused silica substrates and annealed at 800 °C, the respective intensities was found to be about 100:36:40. This suggests that the crystallites of the deposited films have a preferred (110) orientation.

The average crystallite size of the SnO_2 films annealed at different temperatures was calculated from the Scherrer equation (Eq. 1) using the angle position and FWHM of the (110) reflection. As expected, the size of crystallites increased gradually with increasing annealing temperature. The average crystallite size was calculated to be 2.6, 3.9, 5.4, 6.2, 8.9 and 11.1 nm for the annealing temperatures from 300 to 800 °C (step of 100 °C), respectively.

3.4. SEM analysis

Plane views of the SnO_2 films formed on SiO_2/Si substrate after annealing at 300–800 °C are shown in Fig. 5. It was observed that for each annealing temperature, the synthesized films exhibit uniform surface without any significant defects and cracks. Surface of the films consisted of spherical particles fused to each other. Porous and nanosized nature of the films is evident for every

annealing temperature. Although the grain size gradually increases with an increase of annealing temperature the films remain porous. Such porous surface morphology would be an advantage for applications of the films as gas sensors or in optoelectronic devices, due to the large surface area [32]. Thickness of the films was evaluated from the cross-sectional SEM images to be about 160 nm for the 10-layered films.

3.5. AFM analysis

The 3D AFM images of the10-layered SnO_2 films deposited on SiO_2/Si substrates after annealing at 300 and 800 °C are represented in Fig. 6. The images demonstrate considerable changes in a surface morphology caused by annealing. The surface roughness was estimated from calculations of RMS for the area of 1 μm^2. It was found that roughness of the deposited films increases with the annealing temperature. The calculated RMS values ± standard deviation were 0.57±0.04, 0.99±0.04, 1.8±0.1, 2.4±0.1, 3.1±0.1 and 4.0±0.1 for the films annealed in the temperature range from 300 to 800 °C (step of 100 °C), respectively.

3.6. Optical properties

Transmittance spectra of 10-layered SnO_2 films deposited on fused silica substrates recorded in the spectral range of 200–1100 nm are shown in Fig. 7. It is evident that the films are highly transparent in a visible spectral range irrespective of the annealing temperature. The minimal transmittance of 85% and the maximal one of 94% were observed. A strong light absorption in the UV region is attributed to optical band gap energy of SnO_2 thin films. The band gap energy is related to the absorption due to the electron transitions from the valence to the conduction band. According to the data of transmittance spectra, the optical band gap (E_g) of the synthesized SnO_2 films can be calculated using the following equation:

$$h\nu\alpha = C(h\nu - E_g)^n \quad (2)$$

Here $h\nu$ is the photon energy, α is the absorption coefficient, and C is constant. The value of the exponent n denotes the nature of the sample transition. Since SnO_2 is known to be a direct transition semiconductor, n = ½ was chosen for calculations. A Tauc plot, i.e., a graph of $(\alpha h\nu)^2$ vs. photon

energy used for the determination of the direct allowed band gap is represented in inset of Fig. 7. The band gap values were calculated using a linear fit for the straight interval in the region of the largest exponential growth; the intercept with the energy axis corresponded to the optical band gap value. The calculated band gap values were 4.00, 3.92, 3.91, 3.90, 3.88 and 3.86 eV for the SnO_2 films annealed at temperatures from 300 to 800 °C (step of 100 °C), respectively. The obtained values show a blue shift from the gap energy of bulk SnO_2 (3.6 eV). This can be explained by quantum confinement effect, which is expected in semiconducting nanostructures. In semiconductors band gap energies have been found to be particle size dependent. The band gap increases with decreasing of particle size, and the absorption edge is shifted to a higher energy concomitantly [33]. It is seen that the band gap of synthesized SnO_2 films gradually shifts toward the value for the bulk SnO_2 with increasing of annealing temperature. The elevated temperature leads to better crystallinity, reduces grain boundary area and defect concentration. Such behavior associated with quantum confinement effect in SnO_2 nanostructures was previously reported by other researchers [34, 35].

4. Conclusions

Organic-free, simple, fast and cost-effective procedure for the deposition of SnO_2 thin films have been suggested. Highly transparent, porous, nanostructured, continuous films were formed on SiO_2/Si and fused silica substrates. The thickness of the multilayered films after 10 deposition cycles was about 160 nm. Roughness of the films was found to be gradually increasing from 0.57±0.04 to 4.0±0.1 as the annealing temperature is increased from 300 to 800 °C. Regardless the annealing temperature, the deposited films were highly transparent in a visible spectral range with the minimal transmittance of 85%. The optical band gap was found to be grain-size dependent and slightly decreasing with the increasing annealing temperature. The calculated band gap values were in the range from 4.00 to 3.86 eV for the films annealed at temperatures from 300 to 800 °C, respectively.

References

[1] L. Alinauskas, E. Brooke, A. Regoutz, A. Katelnikovas, R. Raudonis, S. Yitzchaik, D.J. Payne, E. Garskaite, Nanostructuring of SnO_2 via solution-based and hard template assisted method, Thin Solid Films, 626 (2017) 38-45.

[2] P. Zhou, J. Wu, Y. Tu, M. Zhen, J. Huo, Y. Wei, Z. Lan, Tin oxide nanosheets as efficient electron transporting materials for perovskite solar cells, Sol. Energy, 137 (2016) 579-584.

[3] N. Yamazoe, K. Suematsu, K. Shimanoe, Surface chemistry of neat tin oxide sensor for response to hydrogen gas in air, Sens. Actuators B, 227 (2016) 403-410.

[4] X. Zhang, G. Xu, Z. Chen, H. Cui, Z. Zhang, X. Zhan, Solvothermal preparation and gas sensing properties of hierarchical pore structure SnO_2 produced using grapefruit peel as a bio-template, Ceram. Int., 43 (2017) 4112-4118.

[5] A.M. Al-Hamdi, U. Rinner, M. Sillanpää, Tin dioxide as a photocatalyst for water treatment: A review, Process Saf. Environ. Prot., 107 (2017) 190-205.

[6] R. Andre, F. Natalio, M.N. Tahir, R. Berger, W. Tremel, Self-cleaning antimicrobial surfaces by bio-enabled growth of SnO_2 coatings on glass, Nanoscale, 5 (2013) 3447-3456.

[7] X. Liu, J. Zhang, W. Si, L. Xi, S. Oswald, C. Yan, O.G. Schmidt, High-rate amorphous SnO_2 nanomembrane anodes for Li-ion batteries with a long cycling life, Nanoscale, 7 (2015) 282-288.

[8] Z. Li, Y. Tan, X. Huang, W. Zhang, Y. Gao, B. Tang, Three-dimensionally ordered macroporous SnO_2 as anode materials for lithium ion batteries, Ceram. Int., 42 (2016) 18887-18893.

[9] H.S. Lee, S.I. Woo, Nanometer-thick amorphous-SnO_2 layer as an oxygen barrier coated on a transparent AZO electrode, Electron. Mater. Lett., 12 (2016) 499-505.

[10] L. Abello, B. Bochu, A. Gaskov, S. Koudryavtseva, G. Lucazeau, M. Roumyantseva, Structural characterization of nanocrystalline SnO_2 by X-ray and Raman spectroscopy, J. Solid State Chem., 135 (1998) 78-85.

[11] A. Yamaguchi, T. Iimura, K. Hotta, N. Teramae, Transparent nanoporous tin-oxide film electrode fabricated by anodization, Thin Solid Films, 519 (2011) 2415-2420.

[12] J. Huang, L. Wang, C. Gu, Z. Wang, Y. Sun, J.-J. Shim, Preparation of porous SnO_2 microcubes and their enhanced gas-sensing property, Sens. Actuators B, 207, Part A (2015) 782-790.

[13] T. Indira Gandhi, R. Ramesh Babu, K. Ramamurthi, M. Arivanandhan, Effect of Mn doping on the electrical and optical properties of SnO_2 thin films deposited by chemical spray pyrolysis technique, Thin Solid Films, 598 (2016) 195-203.

[14] D.V. Nazarov, M.Y. Maximov, P.A. Novikov, A.A. Popovich, A.O. Silin, V.M. Smirnov, N.P. Bobrysheva, O.M. Osmolovskaya, M.G. Osmolovsky, A.M. Rumyantsev, Atomic layer deposition of tin oxide using tetraethyltin to produce high-capacity Li-ion batteries, J. Vac. Sci. Technol. A, 35 (2017) 11.

[15] C. Kim, S. Kim, S.E. Kim, Transparent SnO_x thin films fabricated by radio frequency reactive sputtering with a SnO/Sn composite target, Thin Solid Films, 634 (2017) 175-180.

[16] S.M. Ingole, S.T. Navale, Y.H. Navale, D.K. Bandgar, F.J. Stadler, R.S. Mane, N.S. Ramgir, S.K. Gupta, D.K. Aswal, V.B. Patil, Nanostructured tin oxide films: Physical synthesis, characterization, and gas sensing properties, J. Colloid Interface Sci., 493 (2017) 162-170.

[17] S. Yu, W. Zhang, L. Li, D. Xu, H. Dong, Y. Jin, Fabrication of p-type SnO_2 films via pulsed laser deposition method by using Sb as dopant, Appl. Surf. Sci., 286 (2013) 417-420.

[18] T. Abendroth, B. Schumm, S.A. Alajlan, A.M. Almogbel, G. Mäder, P. Härtel, H. Althues, S. Kaskel, Optical and thermal properties of transparent infrared blocking antimony doped tin oxide thin films, Thin Solid Films, 624 (2017) 152-159.

[19] R. Djamil, K. Aicha, A. Souifi, D. Fayçal, Effect of annealing time on the performance of tin oxide thin films ultraviolet photodetectors, Thin Solid Films, 623 (2017) 1-7.

[20] M.P.S. Rana, F. Singh, K. Joshi, S. Negi, R.C. Ramola, Influence of electronic excitations on structural, optical and electrical properties of undoped and antimony doped tin oxide thin films, Thin Solid Films, 616 (2016) 34-42.

[21] Y.C. Goswami, V. Kumar, P. Rajaram, V. Ganesan, M.A. Malik, P. O'Brien, Synthesis of SnO_2 nanostructures by ultrasonic-assisted sol–gel method, J. Sol-Gel Sci. Technol., 69 (2014) 617-624.

[22] T.J. Liu, Z.G. Jin, L.R. Feng, T. Wang, Conducting antimony-doped tin oxide films derived from stannous oxalate by aqueous sol–gel method, Appl. Surf. Sci., 254 (2008) 6547-6553.

[23] T. Liu, Z. Jin, J. Yang, L. Feng, Preparation and process chemistry of SnO_2 films derived from SnC_2O_4 by the aqueous sol–gel method, J. Am. Ceram. Soc., 91 (2008) 1939-1944.

[24] W. Luo, J. Deng, Q. Fu, D. Zhou, Y. Hu, S. Gong, Z. Zheng, Nanocrystalline SnO_2 film prepared by the aqueous sol–gel method and its application as sensing films of the resistance and SAW H_2S sensor, Sens. Actuators B, 217 (2015) 119-128.

[25] A. Stanulis, A. Hardy, C. De Dobbelaere, J. D'Haen, M. Van Bael, A. Kareiva, SnO_2 thin films from an aqueous citrato peroxo Sn(IV) precursor, J. Sol-Gel Sci. Technol., 62 (2012) 57-64.

[26] A. Stanulis, S. Sakirzanovas, M. Van Bael, A. Kareiva, Sol–gel (combustion) synthesis and characterization of different alkaline earth metal (Ca, Sr, Ba) stannates, J. Sol-Gel Sci. Technol., 64 (2012) 643-652.

[27] J. Rodríguez-Carvajal, Recent advances in magnetic structure determination by neutron powder diffraction, Physica B: Condens. Matter, 192 (1993) 55-69.

[28] D.Y. Chung, E.H. Kim, Y.J. Shin, J.H. Yoo, C.S. Choi, J.D. Kim, Decomposition of oxalate by hydrogen peroxide in aqueous solution, J. Radioanal. Nucl. Chem.-Lett., 201 (1995) 495-507.

[29] E.H. Kim, D.K. Chung, J.H. Park, J.H. Yoo, Dissolution of oxalate precipitate and destruction of oxalate ion by hydrogen peroxide in nitric acid solution, J. Nucl. Sci. Technol., 37 (2000) 601-607.

[30] R. Alcantara, F.J.F. Madrigal, P. Lavela, C. Perez-Vicente, J.L. Tirado, Tin oxalate as a precursor of tin dioxide and electrode materials for lithium-ion batteries, J. Solid State Electrochem., 6 (2001) 55-62.

[31] G.J. McCarthy, J.M. Welton, X-Ray diffraction data for SnO_2. An illustration of the new powder data evaluation methods, Powder Diffr., 4 (1989) 156-159.

[32] Z. Li, Q. Zhao, W. Fan, J. Zhan, Porous SnO_2 nanospheres as sensitive gas sensors for volatile organic compounds detection, Nanoscale, 3 (2011) 1646-1652.

[33] F. Gu, S.F. Wang, M.K. Lü, G.J. Zhou, D. Xu, D.R. Yuan, Photoluminescence properties of SnO_2 nanoparticles synthesized by sol−gel method, J. Phys. Chem. B, 108 (2004) 8119-8123.

[34] G. Pang, S. Chen, Y. Koltypin, A. Zaban, S. Feng, A. Gedanken, Controlling the particle size of calcined SnO_2 nanocrystals, Nano Lett., 1 (2001) 723-726.

[35] L. Shi, H. Lin, Preparation of band gap tunable SnO_2 nanotubes and their ethanol sensing properties, Langmuir, 27 (2011) 3977-3981.

Figure captions

Fig. 1. TG-DSC curves of the dried SnO_2 precursor solution.

Fig. 2. GIXRD patterns of the 10-layered SnO_2 films annealed at different temperatures. The 2theta range of 53–57° with a strong diffraction peak from the substrate is excluded for convenience.

Fig. 3. Rietveld refinement of the XRD data on the SnO_2 samples annealed at 800 °C: powders (a) and film (b). The open cycles and solid line (red) represent the experimental and calculated intensities, respectively; the line below (blue) is the difference between them. Tick marks (green) indicate the positions of Bragg peaks in the $P4_2/mnm$ space group.

Fig. 4. Dependence of the lattice parameters on the annealing temperature.

Fig. 5. SEM images of the SnO_2 films annealed at 300 (a), 400 (b), 500 (c), 600 (d), 700 (e) and 800 °C (f).

Fig. 6. 3D AFM images of the SnO_2 films annealed at 300 (a) and 800 °C (b).

Fig. 7. Transmittance spectra of the 10-layered SnO_2 films annealed at different temperatures. *Inset:* Tauc plot for the determination of the direct allowed band gap.

Highlights

- Highly transparent porous SnO_2 films were fabricated at 300–800 ºC temperature
- The entire deposition process requires neither organic solvents nor complexing agent
- The films exhibit a preferred (110) orientation of the crystallites
- Roughness of the films increased with increasing of annealing temperature
- Optical band gap was found to be slightly dependent on the annealing temperature

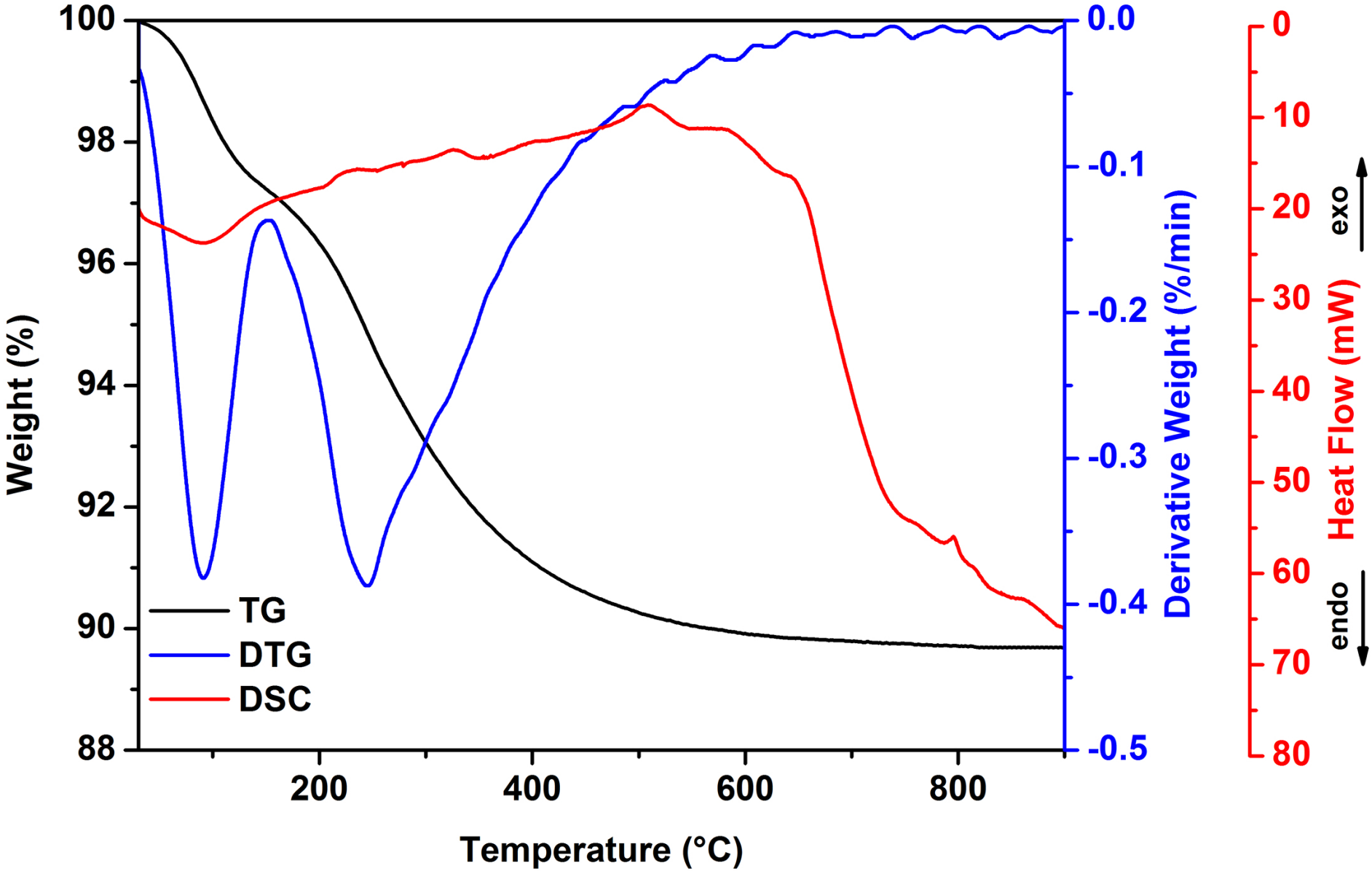
100
98
96
94
92
90
88
Weight (%)
200
400
600
800
Temperature (°C)
TG
DTG
DSC
0.0
-0.1
-0.2
-0.3
-0.4
-0.5
Derivative Weight (%/min)
0
10
20
30
40
50
60
70
80
Heat Flow (mW)
exo
endo

Figure 1

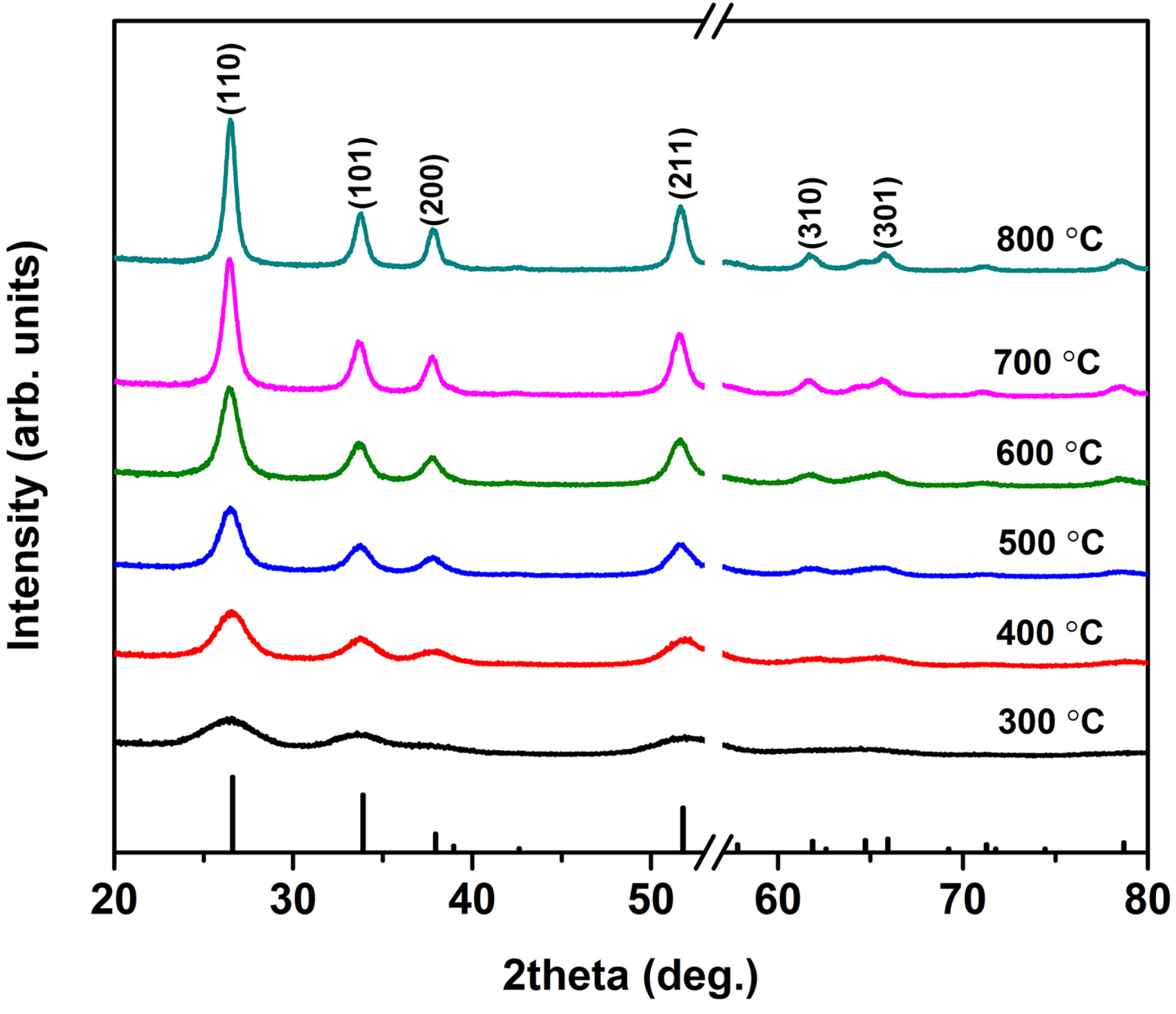
(110)
(101)
(200)
(211)
(310)
(301)
800 °C
700 °C
600 °C
500 °C
400 °C
300 °C
Intensity (arb. units)
20
30
40
50
60
70
80
2theta (deg.)

Figure 2

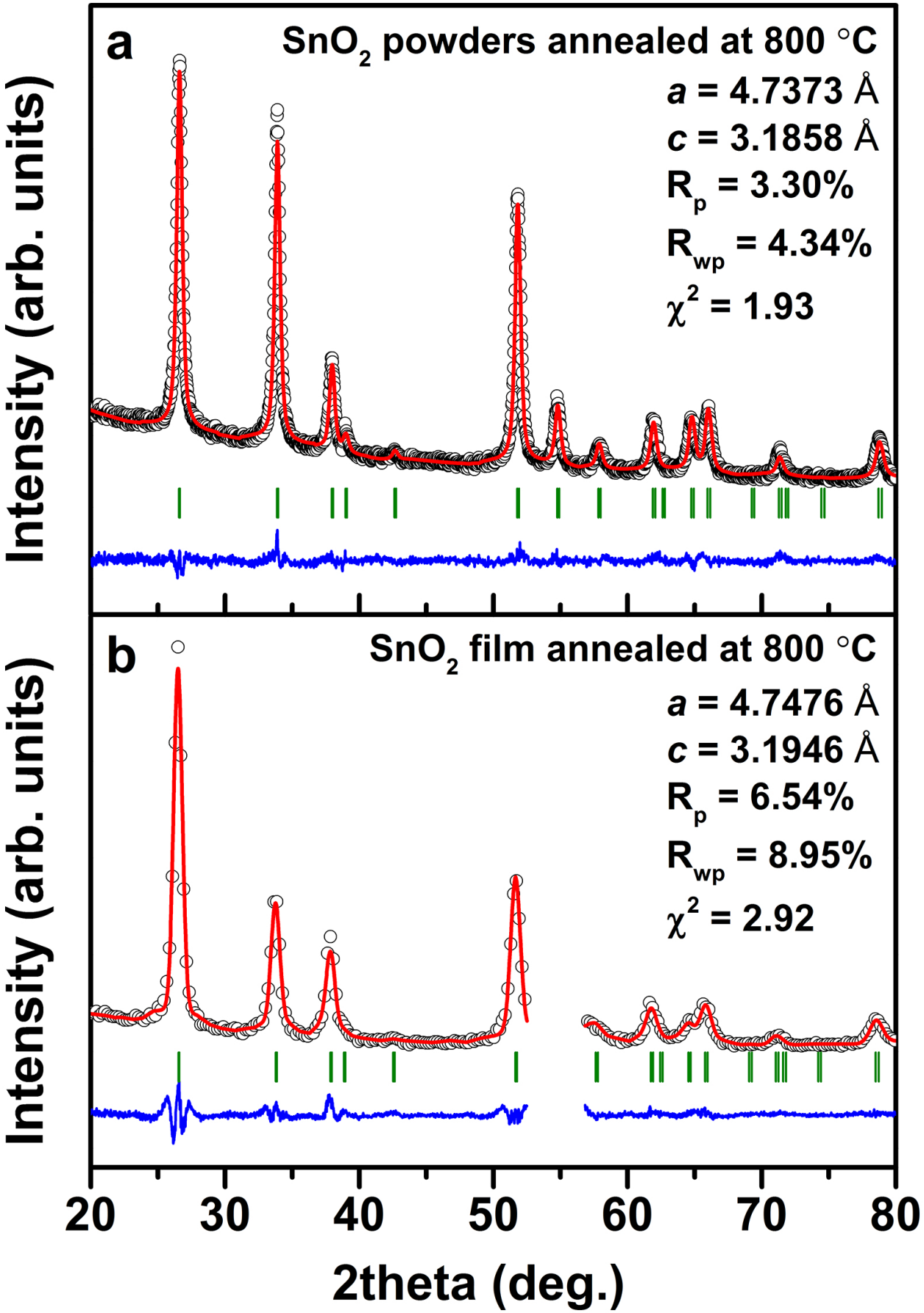
a
SnO2 powders annealed at 800 °C
a = 4.7373 Å
c = 3.1858 Å
Rp = 3.30%
Rwp = 4.34%
χ2 = 1.93
b
SnO2 film annealed at 800 °C
a = 4.7476 Å
c = 3.1946 Å
Rp = 6.54%
Rwp = 8.95%
χ2 = 2.92
Intensity (arb. units)
Intensity (arb. units)
20
30
40
50
60
70
80
2theta (deg.)

Figure 3

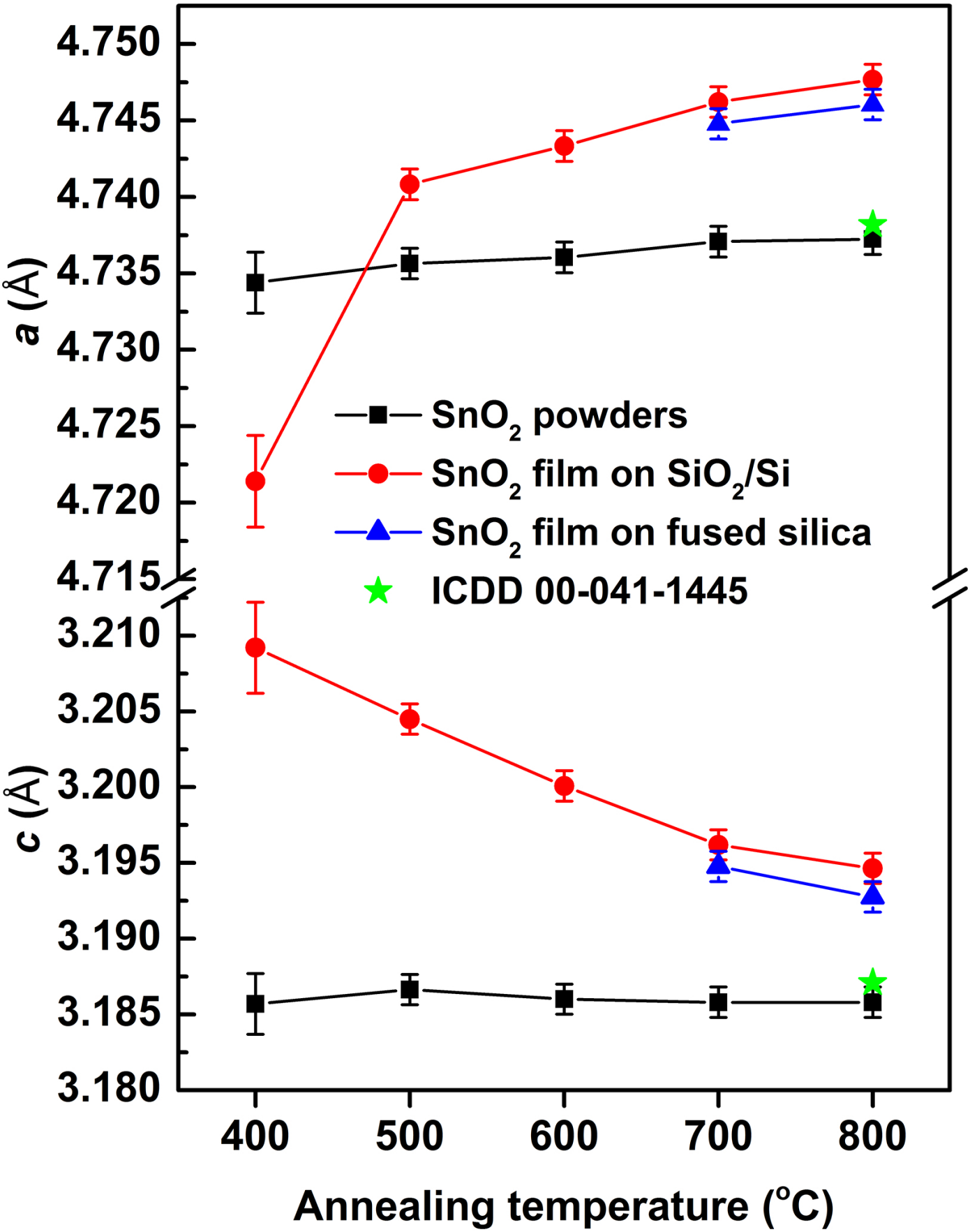
4.750
4.745
4.740
4.735
4.730
4.725
4.720
4.715
a (Å)
3.210
3.205
3.200
3.195
3.190
3.185
3.180
c (Å)
400
500
600
700
800
Annealing temperature (°C)
SnO2 powders
SnO2 film on SiO2/Si
SnO2 film on fused silica
ICDD 00-041-1445

Figure 4

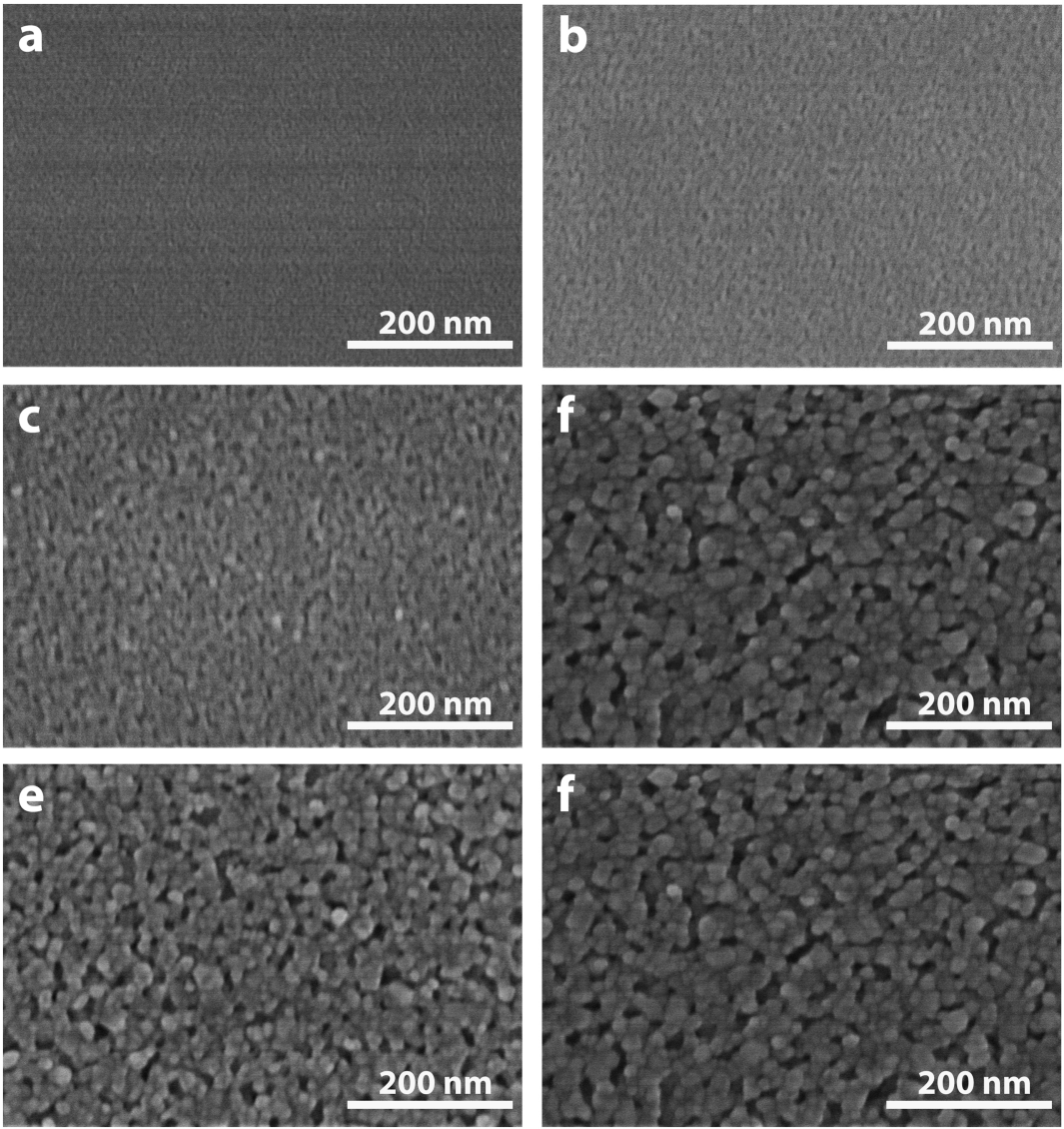

Figure 5

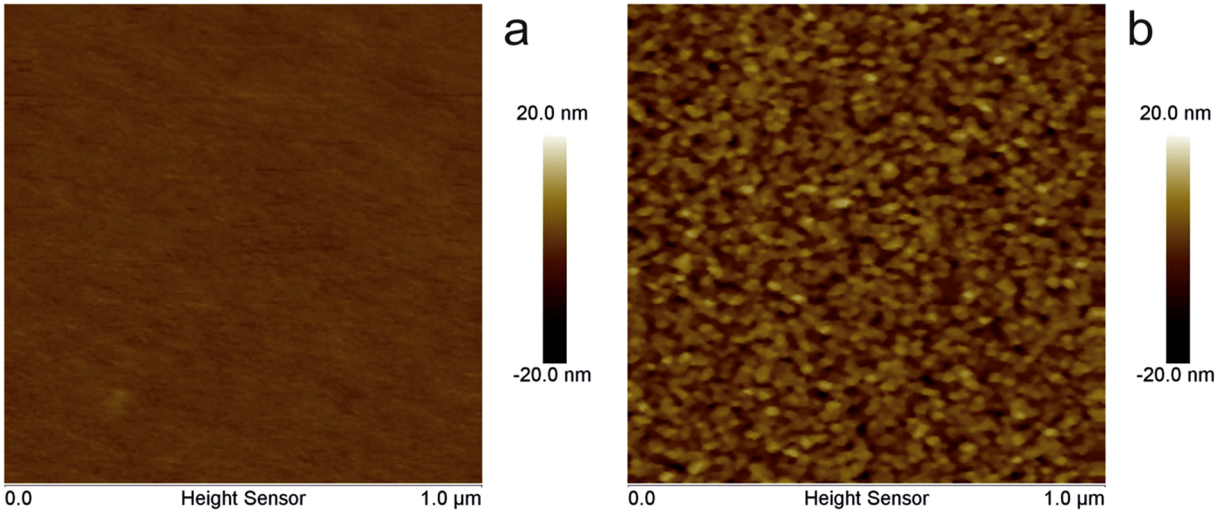
a
20.0 nm
-20.0 nm
0.0
Height Sensor
1.0 µm
b
20.0 nm
-20.0 nm
0.0
Height Sensor
1.0 µm

Figure 6

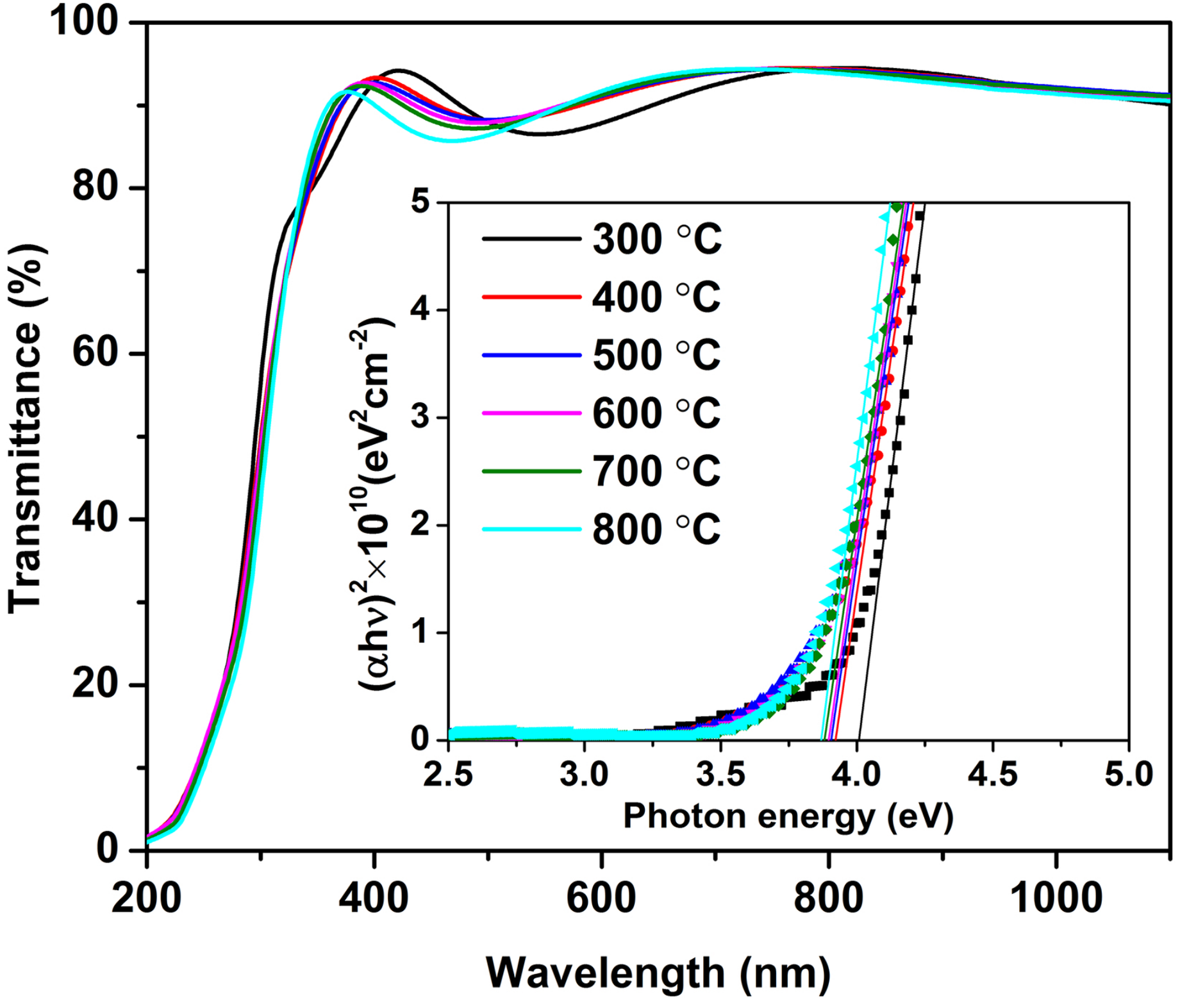
Transmittance (%)
Wavelength (nm)
100
80
60
40
20
0
200
400
600
800
1000
$(\alpha h\nu)^2 \times 10^{10} (eV^2 cm^{-2})$
Photon energy (eV)
5
4
3
2
1
0
2.5
3.0
3.5
4.0
4.5
5.0
300 °C
400 °C
500 °C
600 °C
700 °C
800 °C

Figure 7